Effect of Thermomechanical Processing on the Microstructure, Properties, and Work Behavior of a $Ti_{50.5}Ni_{29.5}Pt_{20}$ High-Temperature Shape Memory Alloy

Ronald Noebe, Susan Draper, Darrell Gaydosh, Anita Garg, Brad Lerch, Nicholas Penney, Glen Bigelow, and Santo Padula, II
NASA Glenn Research Center, Cleveland, OH., USA

Jeff Brown
Dynalloy, Inc., Costa Mesa, CA., USA

Abstract

TiNiPt shape memory alloys are particularly promising for use as solid state actuators in environments up to 300 °C, due to a reasonable balance of properties, including acceptable work output. However, one of the challenges to commercializing a viable high-temperature shape memory alloy (HTSMA) is to establish the appropriate primary and secondary processing techniques for fabrication of the material in a required product form such as rod and wire. Consequently, a $Ti_{50.5}Ni_{29.5}Pt_{20}$ alloy was processed using several techniques including single-pass high-temperature extrusion, multiple-pass high-temperature extrusion, and cold drawing to produce bar stock, thin rod, and fine wire, respectively. The effects of heat treatment on the hardness, grain size, room temperature tensile properties, and transformation temperatures of hot- and cold-worked material were examined. Basic tensile properties as a function of temperature and the strain-temperature response of the alloy under constant load, for the determination of work output, were also investigated for various forms of the $Ti_{50.5}Ni_{29.5}Pt_{20}$ alloy, including fine wire.

Introduction

The unique behavior of TiNi and related shape memory alloys is based on a reversible, temperature-dependent, austenite-to-martensite phase transformation. This reversible behavior is the basis for such properties as superelasticity and shape memory effect, which is the recovery of low temperature deformation in the material simply by heating the alloy through its phase transformation. Additionally, some alloys that display shape memory effect can recover their original shape even when a substantial opposing force is applied to the material. Under such conditions of load-biased recovery, the alloy would perform work, thus, acting as a solid state actuator. TiNi, in particular, is capable of specific work output with equivalent or higher energy density than pneumatic actuators or D.C. motors [1].

Due to a limited range in transformation temperatures, generally between -100 to 100 °C [2], the unique properties of TiNi alloys can only be exploited in applications near room temperature. However, a material with properties similar to TiNi, including high specific work output with good dimensional stability, but with transformation temperatures greater than 100°C, would open up new applications for shape memory alloys in the aerospace, automotive, automation and controls, and numerous other industries.

Alloying additions to TiNi are primarily used to affect changes in the transformation temperatures of the resulting material: either to increase or decrease the transformation temperatures or change the width of the hysteresis. It is has been known for some time that additions of Pd, Pt, and Au, substituted for Ni or Hf and Zr substituted for Ti can effectively raise the transformation temperature of TiNi. However, actual research demonstrating the useful work characteristics of these HTSMA is a rather recent and limited activity. Useful work characteristics have been verified in TiNiHf thin films [3,4] and bulk TiNiPt [5] and TiNiPd [6] alloys. Therefore, at least the possibility of developing high-temperature shape memory alloys, specifically for actuator type applications, seems plausible.

Pt additions are the most effective in raising the transformation temperature of TiNi with a martensite start temperature (M_s) ranging from -10 °C (10 at.% Pt) to nearly 1050°C (50 at.% Pt) [7,8]. But until recently, research on TiNiPt alloys had been limited to the stress-free shape recovery of a $Ti_{50}Ni_{30}Pt_{20}$ alloy (confirming the thermoelastic nature of the phase transformation in this system) [7], and a few room temperature tensile tests of alloys with various Pt contents [7,9]. However, recent work by Noebe et al. [5] has demonstrated that the $Ti_{50}Ni_{30}Pt_{20}$ alloy was also capable of significant work output (8.7 J/cm^3), and that the strain-temperature response of the material under stresses up to at least 257 MPa occurred without any significant plastic deformation. This alloy also has a reasonable balance of mechanical properties [10] and adequate oxidation resistance for long-term exposure up to 600 °C [11].

Once a viable HTSMA has been identified, the next major step in the maturation of these materials is to develop the processing procedures by which they can be produced into a product form such as rod or wire, for the fabrication of

various demonstration articles. This would include primary thermomechanical processes for breaking down ingots into rod and wire and secondary processes such as annealing and additional thermomechanical treatments used to further optimize and refine basic mechanical and shape-memory-related properties. Consequently, the microstructure, tensile properties, and work characteristics of a $Ti_{50.5}Ni_{29.5}Pt_{20}$ alloy were determined for various product forms including bar, rod, and fine wire, after certain combinations of primary processing, annealing, and additional thermomechanical treatment. Preliminary results are presented in this paper.

Material Processing

A target composition of $Ti_{50.5}Ni_{29.5}Pt_{20}$ (all compositions are noted in atomic percent) was chosen for investigation because it was originally believed that the slight Ti-rich composition would help ensure high transformation temperatures. While such caution is warranted for binary TiNi [2], TiNiHf [12], and TiNiPd [13] alloys, subsequent research indicated that transformation temperatures do not drop off precipitously in the TiNiPt system as the composition becomes Ti-lean [8], in stark contrast to the other systems previously mentioned.

Nevertheless, three slightly Ti-rich ingots were prepared by vacuum induction melting of high purity elemental constituents (99.95 Ti, 99.995 Pt, 99.98 Ni) using a graphite crucible. The induction furnace was equipped with tilt-pour capability and the melts were cast into a cylindrical copper mold 25.4 mm diameter by 102 mm length, with an appropriate hot top to accommodate shrinkage during solidification. Prior to thermomechanical processing, the ingots were homogenized in a vacuum furnace at 1050 °C for 72 hr. The ingots were subsequently placed into steel extrusion cans, which were evacuated and sealed.

Ext29 – 5 mm Diameter Bar
One ingot (Ext29) was extruded at 900 °C in a single pass resulting in an approximately 5 mm diameter bar. Cylindrical dog-bone-shaped tensile samples 50.8 mm long with threaded button ends and a 17.4 mm long by 3.81 mm diameter gage section were machined from the bar using a CNC lathe. In this particular case, all tensile samples were given a stress relief heat treatment at 600 °C for 30 min. followed by a furnace cool prior to testing. The function of this heat treatment was to relieve any residual stresses introduced during the extrusion and machining processes.

Ingot B3 – 1.1 mm Diameter Rod
The remaining two ingots were repeatedly hot extruded at 927°C to create thin rods. To prevent Fe contamination of the $Ti_{50.5}Ni_{29.5}Pt_{20}$ alloy, the extrusion can was removed by pickling after each extrusion run and the shape memory alloy was placed into a new extrusion can subsequent to the next extrusion cycle. In this manner, Ingot B3 was reduced in diameter from 25.4 mm to 1.5 mm. This rod was then centerless ground to a final diameter of 1.1 mm to remove the majority of the corrosion products and surface damage due to the pickling process. Subsequently, the rod was annealed at 600° C for 30 min. The 1.1 mm rod was mechanically tested in the as-annealed condition similar to Ext29, but as straight rod with no reduced gage section.

Ingot B1 – 1.5 mm Diameter rod & 0.5 mm Diameter Wire
Ingot B1 was reduced in diameter to 2.2 mm by the same multiple hot extrusion process as that described for ingot B3, and then centerless ground to a diameter of 1.5 mm. A part of the 1.5 mm rod was then tensile tested at room temperature and the balance of the material was subsequently cold drawn to a final diameter of 0.5mm. The final draw pass left the material with 35% cold work. Both the 1.5 mm rod and 0.5 mm diameter wire were characterized in the as-processed (hot or cold worked) condition and after annealing at temperatures between 400 and 900 °C followed by air cooling.

Experimental Procedures

Material Characterization
After final processing, the chemical composition was determined for all three ingots by inductively coupled plasma spectroscopy, and by conventional nitrogen/oxygen and carbon/sulfur determination. The microstructure of the $Ti_{50.5}Ni_{29.5}Pt_{20}$ alloy after various mechanical and thermal processing treatments was examined by optical microscopy of polished and etched samples to facilitate grain size measurements, and by conventional scanning electron microscopy (SEM) and transmission electron microscopy techniques (TEM) to identify the type, size, and distribution of all phases present in the material. Finally, x-ray analysis was used to confirm the structure and determine the lattice parameters of the martensite phase.

Microhardness measurements were made on mounted and polished samples using a Vickers indenter, with a 500 g load and dwell time of 10 s. A minimum of 5 measurements were made at random locations within the interior section of the sample to generate a statistically significant mean hardness.

Transformation temperatures for the wire were determined by high resolution resistivity measurements as described in reference [6]. Transformation temperatures for the bar and rod were determined by measuring the strain-temperature response of the material under essentially zero load (stress-free condition) using the mechanical test setup described below. It has been previously demonstrated that as long as thermocouples are spot welded directly to the sample, both processes provide identical results [6].

Mechanical Testing
Mechanical testing of the 5 mm bar and the 1.1 mm rod was performed using a servo-hydraulic load frame equipped with a digital controller. Strain measurements were taken with a 12.7 mm gage length extensometer. The extensometer had a maximum range of +20/-10 % strain and was equipped with 85 mm long alumina probes with a v-chisel edge. Both the bar and rod samples were induction heated and all temperatures were measured with K-type thermocouples, which were spot-welded directly to the sample. Temperature gradients across

Table 1: Transformation temperatures for various forms of a $Ti_{50.5}Ni_{29.5}Pt_{20}$ alloy.

Material Form	Condition	A_s (°C)	A_f (°C)	M_s (°C)	M_f (°C)	Hysteresis ($A_f - M_s$)	Technique
5 mm bar	Annealed*	299	337	322	274	15	Dilatometry
1.1 mm rod	Annealed*	297	326	309	277	17	Dilatometry
0.5 mm wire	Cold Drawn	238	275	259	201	16	Resistivity
0.5 mm wire	Annealed*	270	296	285	251	11	Resistivity

*Annealed 30 min at 600 °C

the sample gage section were calibrated to within ± 0.5% of the test temperature.

Monotonic tensile tests for the 5 mm bar and the 1.1 mm rod were performed at various temperatures. Tests were run in strain control to failure at a rate of 1×10^{-4} sec^{-1}. The work characteristics of these materials were determined from constant load, strain versus temperature tests (referred to as load-bias tests). Specimens were strained at room temperature to the required load in strain control at a rate of 1×10^{-4} sec^{-1}. At this point the controller was switched to load control to maintain the desired load. Specimens were then thermally cycled twice from room temperature to about 100 ºC above the austenite finish temperature (A_f). Heating rates were maintained at 10 ºC/min. The load bias tests were run in a series of increasing loads on the same sample, where the specimen was unloaded at room temperature and then strained again to the next higher load level, at which point the thermal cycling process was repeated. The specific work output of the alloy was determined by measuring the resultant change in strain during the martensite-to-austenite transformation during the second heating cycle and multiplying it by the stress applied during the thermal cycle. Additional details can be found in references [5,6].

Room temperature tensile tests for the 1.5 mm rod and 0.5 mm diameter $Ti_{50.5}Ni_{29.5}Pt_{20}$ wire were performed using a screw-driven load frame using wedge grips and operating in strain control at a rate of 1×10^{-4} sec^{-1}. Total sample length was 63.5 mm and strain was measured over the central section of the sample using a 12.7 mm extensometer.

Finally, the work characteristics of the 0.5 mm wire were determined by dead weight loading and repeated heating of the material through its transformation temperatures. This was accomplished by attaching the HTSMA wire to the center of a pulley system anchored at one end and connected to a free-hanging weight pan at the other. Certified weights were added to the pan to achieve the various load levels. The HTSMA wire was electrically insulated from the rest of the system and was direct resistance heated by running a current through the wire using a direct current power supply. The power supply was interfaced with a computer using dSpace/Matlab to control the current/time cycle (or heating cycle) and the number of cycles. The strain-time response of the wire under load was measured using a pair of laser extensometers, also interfaced with the computer system for automatic data acquisition over many cycles.

Results & Discussion

Material Characterization

A total of three ingots, with the same aim composition, were cast, homogenized, and thermomechanically processed for use in this study. The compositional measurements were very consistent averaging 50.2 ± 0.1 at.% Ti, 29.4 ± 0.2 at.% Ni, 19.7 ± 0.1 at.% Pt, 0.37 ± 0.15 at.% C, and 0.33 ± 0.06 at.% O for the three ingots. Within the resolution of the chemical measurement techniques (± 0.5% of the absolute value of the constituent), none of the individual ingots were discernibly different in composition from each other or from the aim composition. In addition, oxygen and carbon (due to the use of graphite crucibles) were present in all the ingots at similar levels.

The microstructures of the $Ti_{50.5}Ni_{29.5}Pt_{20}$ alloy as a function of thermomechanical processing are shown in Figs. 1-3. In general, the materials were predominantly single phase martensite at room temperature but also contained several volume percent total of additional phases. X-ray diffraction was used to confirm that the martensite phase was the B19 (orthorhombic) phase, which is typically observed in TiNi alloys containing high levels of Pt or Pd. [7]. The lattice parameters for the martensite phase were determined to be a_o = 0.275 nm, b_o = 0.444 nm, and c_o = 0.470 nm. Scanning and transmission electron microscopy were used to identify the additional phases. There were two kinds of particles present; an intermetallic phase containing Ti, Ni, and Pt and the other containing a high amount of Ti with C and O. The intermetallic phase was an FCC structured $Ti_2(Ni,Pt)$ or $Ti_4(Ni,Pt)_2O$ phase with a lattice parameter a_o = 1.16 nm. This intermetallic phase is isostructural to the Ti_2Ni or Ti_4Ni_2O phase commonly observed in TiNi alloys and is believed to be stabilized by oxygen. For convenience we will refer to this phase as $Ti_2(Ni,Pt)$. The other phase present was an FCC structured, interstitial based titanium carbide or titanium oxy-carbide with a lattice parameter a_o = 0.44 nm. The $Ti_2(Ni,Pt)$ phase was blocky in morphology and ranged in size from 1-4 μm, whereas the carbide particles ranged in size from about 0.5 to 2 μm. The total volume fraction of all second phase particles in a given ingot was less than 3%.

The 5 mm bar produced by simple extrusion (Ext29) had an equiaxed, recrystallized grain structure, with an average grain size of about 10 μm (Fig. 1). The distribution of $Ti_2(Ni,Pt)$ phase was inhomogeneous reflecting the interdendritic nature of this second phase and that a single extrusion pass was not sufficient to completely break up this segregation. However, after multiple extrusion passes, represented by the 1.1 mm bar shown in Fig.2, the same material possessed a more homogeneous distribution of micron size $Ti_2(Ni,Pt)$ and Ti(C,O) particles and a grain size on the order of 2-4 μm. The gray particles in Fig. 2 are the $Ti_2(Ni,Pt)$ phase, the almost spherical black particles are Ti(C,O), and the elongated black shapes in Fig. 2b are actually pores. These pores were due to pullout of the $T_2(Ni,Pt)$ phase during the polishing process. This phase was apparently very brittle and cracks were occasionally found in some of the larger particles. Subsequent cold drawing of the multiple-pass hot extruded rod, represented by the 0.5 mm wire shown in Fig. 3, resulted in further refinement of the microstructure. However, stringers of cracked $Ti_2(Ni,Pt)$ and voids were observed parallel to the drawing direction. These stringers only formed from the $Ti_2(Ni,Pt)$ phase and cracks and voiding were never associated with the carbide phase. In fact, the arrow in Fig. 3 shows a fine stringer of $Ti_2(Ni,Pt)$ bowing out around a carbide particle.

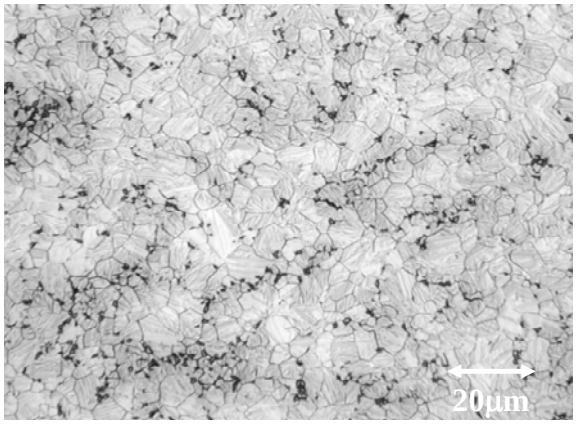

Figure 1: Microstructure of the 5 mm bar (Ext29) etched to reveal grain size and showing an inhomogeneous distribution of $Ti_2(Ni,Pt)$ phase.

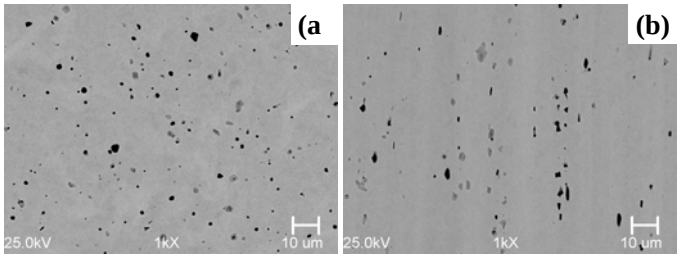

Figure 2: As-polished microstructure of the 1.1 mm bar produced by multiple-pass hot extrusion in the a) transverse and b) longitudinal direction. See text for discussion.

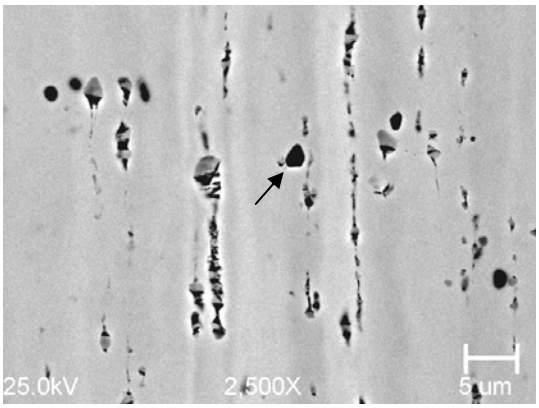

Figure 3: Longitudinal cross-section of the cold-drawn 0.5 mm wire.

The transformation temperatures for various forms of the $Ti_{50.5}Ni_{29.5}Pt_{20}$ alloy are listed in Table 1. The transformation temperatures for the annealed bar and rod were similar and are considerably greater than that of any binary TiNi alloys. The alloy also exhibited a very narrow hysteresis and a transformation span (A_f-M_f) comparable to conventional TiNi alloys. The 0.5 mm wire had transformation temperatures about 20 °C lower than the bar or rod even after a similar annealing treatment but recovered a significant percentage of its maximum transformation temperature compared to the cold-worked wire. Also, all the transformation temperatures listed in Table 1, were thermally stable and did not change with thermal cycling (75-100 cycles) to temperatures as high as 450 °C, including those for the cold worked wire. This thermal stability is due in part to the stability of the microstructure and the fact that the recovery temperature for the alloy is fairly high, as discussed in the following section.

Effect of Annealing on Properties

It is well known that cold work, such as wire drawing, significantly increases the yield strength of a metal but at the expense of ductility. Therefore, it is necessary to anneal most metals after a certain amount of cold work to restore ductility before continuing with the deformation processing of the alloy. Yet, recrystallization with significant grain growth during annealing can make some metals, especially those with BCC or BCC-derivative structures like TiNi and TiNiPt, more difficult to process.

Also, some degree of cold work is extremely beneficial to material properties, particularly for increasing strength. In shape memory alloys, cold work can be used to increase the resistance of the martensite phase to further slip processes. This in turn reduces the amount of plastic deformation or "walking" that occurs when the alloy is cycled under load through its transformation temperatures [2]. However, cold work also severely depresses the transformation temperatures of shape memory alloys; negating some of the high temperature capability that we strive to develop in these materials. Therefore, understanding all the ramifications of this complicated balance between cold work and recovery and its effect on properties is crucial to controlling and optimizing the behavior of shape memory alloys. Keeping this mind, we have investigated the effect of annealing on the hardness, grain size, and transformation temperatures for the $Ti_{50.5}Ni_{29.5}Pt_{20}$ alloy and related materials.

Figure 4 is a plot of hardness as a function of annealing temperature for the $Ti_{50.5}Ni_{29.5}Pt_{20}$ alloy in the hot-worked (1.5mm rod) and cold-drawn condition containing 35% cold work (0.5 mm wire). In addition, similar data for a stoichiometric $Ti_{50}Ni_{30}Pt_{20}$ alloy, also in the form of hot-worked rod or rod containing 10% cold work from swaging, is included in the plot. For an annealing time of 30 minutes, recovery starts at 450 °C and is nearly complete by 600 °C. Even hot-worked rod annealed for only 10 minutes showed a slight recovery in hardness over this temperature range.

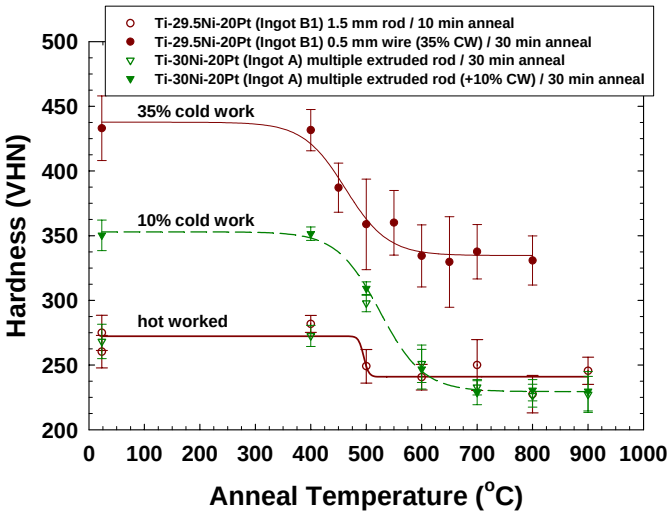

Figure 4: The effect of annealing temperature on the hardness of slightly Ti-rich $Ti_{50.5}Ni_{29.5}Pt_{20}$ and near stoichiometric $Ti_{50}Ni_{30}Pt_{20}$ alloys.

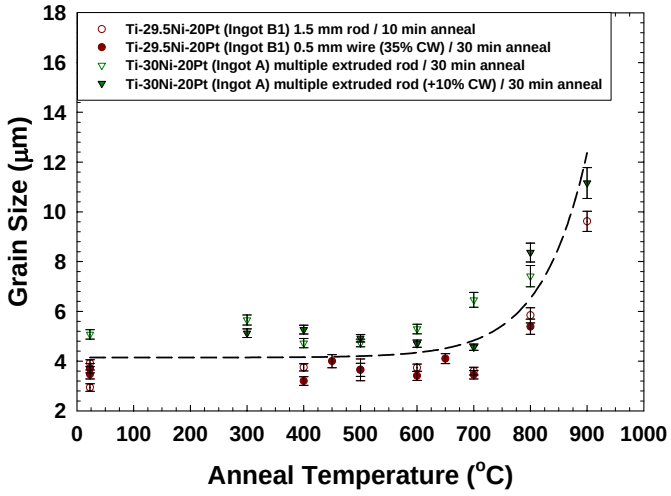

Figure 5: Corresponding grain size as a function of temperature for the same materials shown in Fig. 4.

Figure 5 is the corresponding plot of grain size as a function annealing temperature for the same materials shown in Fig. 4. The multiple-pass hot-extruded rod had a grain size of 2-4 μm, similar to the cold-worked wire. For all materials, grain growth was not observed until an annealing temperature greater than 700 °C. Recrystallization is the nucleation and growth of stress-free grains in the material that nucleate at the boundaries of the polygonized subgrain structure that forms by the end of the recovery process. These new stress-free grains grow at the expense of grains containing much higher levels of internal energy. Since recovery is complete by 700 °C and the first variation in grain size is observed just above that temperature, then recrystallization must begin at or near 700 °C.

The effect of annealing temperature on the transformation temperatures of the 0.5 mm wire with 35% cold work is shown in Fig. 6. Cold work depresses the transformation temperatures for the $Ti_{50.5}Ni_{29.5}Pt_{20}$ alloy, on average by 26 °C, but not uniformly for the various transformation temperatures. Cold work has over twice the effect on the M_f compared to the A_f, as shown in Fig. 6 and Table 1. In all cases, the transformation temperatures increase rapidly with annealing temperature between 500 and 600 °C and are stable and independent of annealing temperature at 700 °C and above, consistent with the recovery and recrystallization behavior of the alloy.

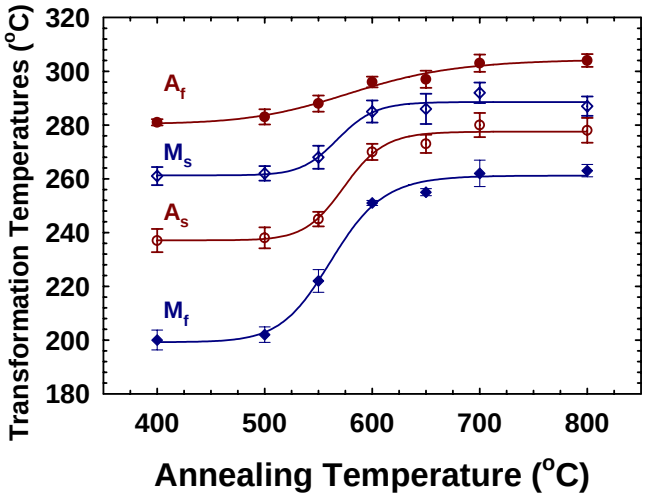

Figure 6: Transformation temperatures for cold worked (35%) $Ti_{50.5}Ni_{29.5}Pt_{20}$ 0.5 mm wire after annealing for 30 min at various temperatures.

Isothermal Tensile Behavior

Room temperature tensile properties for the various forms of the $Ti_{50.5}Ni_{29.5}Pt_{20}$ alloy are summarized in Table 2. The hot worked 1.5 mm rod, and the annealed 1.5 and 1.1 mm rods and 0.5 mm wire all had similar yield stresses. This was due to the similarity in microstructure of the alloy in each case: a recovered microstructure with a 2-4 μm grain size. There was, however, a difference in yield strength between the annealed 5 mm bar and the rod and wire, with the former exhibiting a much lower yield strength. This difference in strength was attributed to the difference in grain size, which was 10 μm for the 5 mm bar compared to 2-4 μm for the rods and wire. It should be noted that the yield strength at room temperature for all these materials represents the stress for the onset of significant twin motion or detwinning. However, the yield stress for both slip and twinning often obey some form of a Hall-Petch relation [14], which would explain the difference in yield strength in this case.

The effect of cold work on properties is dramatically illustrated with the 0.5 mm wire, which shows a four-fold increase in yield strength and a significant decrease in tensile ductility (fracture strain) when 35% cold work is imparted to the material. The 0.5 mm wire also exhibited an extremely high ultimate tensile strength in either condition, in spite of the cracked $Ti_2(Ni,Pt)$ phase. This was probably due to the significant refinement of the microstructure, shown in Fig. 3.

The product forms, other than wire, had similar UTS values and fracture strains, except for the 1.1 mm rod. In this particular case the material was pickled too long after the final extrusion pass and contained significant surface damage. Since the centerless grinder was not capable of grinding finer than 1.1 mm diameter, the majority of the surface pitting and corrosion damage was removed from the rod but some surface defects were still present when these samples were tested, thus providing a worst case scenario for the material. In spite of a poor surface finish or cracked second phase particles (in the case of the wire), the $Ti_{50.5}Ni_{29.5}Pt_{20}$ alloy exhibited much better room temperature tensile ductility than previously reported for stoichiometric $Ti_{50}Ni_{30}Pt_{20}$, which under the best conditions was less than 4% [5,7,9].

Table 2: Average room temperature tensile properties for $Ti_{50.5}Ni_{29.5}Pt_{20}$ in various forms. Annealed samples were tested after heat treatment for 30 min at 600 °C.

Material form / Tensile Properties	Y.S. (MPa)	U.T.S. (MPa)	Fracture Strain (%)
5 mm bar (Ext29) (annealed)	232	1298	11.0
1.1 mm rod (Ingot B3) (annealed)	325	1045	6.5
1.5 mm rod (Ingot B1) (hot-worked)	314	1390	9.0
1.5 mm rod (Ingot B1) (annealed)	305	1259	7.8
0.5 mm wire (Ingot B1) (annealed)	334	1550	8.2
0.5 mm wire (Ingot B1) (35% cold work)	1344	1670	2.7

The stress-strain behavior of the $Ti_{50.5}Ni_{29.5}Pt_{20}$ alloy at various temperatures is shown in Fig. 7 for the 5 mm bar and in Fig. 8 for the 1.1 mm rod. Unlike binary NiTi alloys that often exhibit a stress plateau indicative of detwinning when tested below the M_f, the stress-strain curves for the martensite phase of the $Ti_{50.5}Ni_{29.5}Pt_{20}$ show continuous hardening with increasing strain. However, they did exhibit an initial region of reduced work hardening rate. At temperatures just above the A_f (for example the 350 °C tensile curves in Figs. 7 and 8), the material exhibits a stress plateau and in the case of the 1.1 mm rod a slight yield point, which are due to the formation of stress-induced martensite. Above the M_d temperature, deformation occurs by slip of the austenite phase at a stress much greater than that of the martensite yield but proceeds with a relatively low work hardening rate. At all temperatures investigated, the fine grained 1.1 mm rod was stronger than the 5 mm diameter bar. The most pronounced difference in strength between these two materials occurred for samples tested in the fully austenitic condition where the yield and fracture stresses were nearly 70% greater for the 1.1 mm rod compared to the 5 mm bar.

The tensile yield strength versus temperature behavior for the $Ti_{50.5}Ni_{29.5}Pt_{20}$ bar and rod is plotted in Fig. 9, which also contains data for $Ti_{50}Ni_{30}Pt_{20}$ and binary TiNi alloys. The yield strength versus temperature behavior for the TiNi-20Pt alloys is actually composed of three distinct processes. At temperatures below A_f, the material is martensitic and the yield stress represents the stress at which detwinning begins. In this region the yield stress decreased with increasing temperature reaching a minimum near the A_f. Between the A_f and M_d temperatures, the material was austenitic but yielding was due to the formation of stress-induced martensite. The yield strength for this process increased dramatically with increasing test temperature over this relatively narrow range. At temperatures above about 370 °C, the parent austenite phase deforms by usual slip processes and strength would actually begin to decrease with further increases in test temperature.

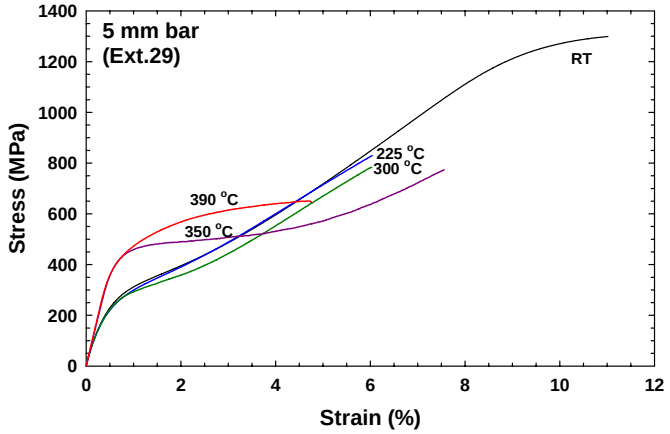

Figure 7: Representative tensile stress-strain curves for the 5 mm diameter bar tested at various temperatures.

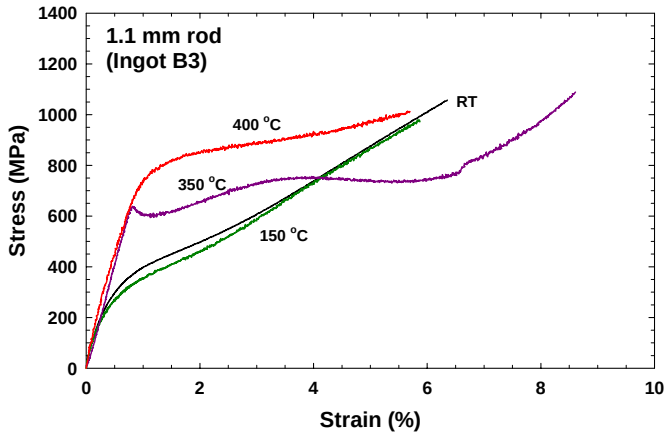

Figure 8: Representative tensile stress-strain curves for the 1.1 mm diameter rod tested at various temperatures.

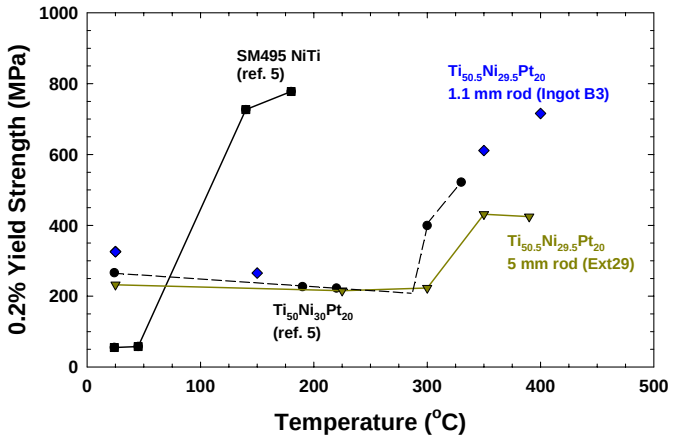

Figure 9: Yield strength as a function of temperature for a conventional TiNi shape memory alloy [5] and TiNi-20Pt HTSMA of Ti-rich (this work) and near stoichiometric [5] composition.

It is clear that both the binary TiNi and TiNi-20Pt alloys show a very distinct and significant increase in yield strength as the temperature increases through the martensite-to-austenite transformation range for each alloy. However, the yield strength of the martensite phase in the TiNi-20Pt alloys is 4-6 times greater than that of binary TiNi, indicating that detwinning is much more difficult in these highly alloyed materials containing substantial amounts of Pt.

Constant-Load, Strain-Temperature Testing and Work Output

The principal application for high-temperature shape memory alloys such as TiNiPt would be for use as solid state actuators, where work output (or the ability of the material to recover strain against some biasing force) is the primary consideration. Consequently, load-bias testing was performed to quantify the work output of the $Ti_{50.5}Ni_{29.5}Pt_{20}$ alloy in its various forms as a function of applied stress. Specific thermomechanical treatments to optimize the work capability and improve the dimensional stability of the alloy during load-biased thermal cycling were also attempted and these results are discussed in the following section.

For the constant-load, strain-temperature testing, the load was applied to the sample at room temperature and then held constant as the sample was heated and cooled through the transformation. During this process, the strain in the sample due to the initial applied load at room temperature, prior to any thermal cycling, was always much smaller than when the sample was cooled through the transformation while under load. As a result, the transformation strain during the initial heating cycle was also much smaller than in successive cycles. This type of behavior is quite common in conventional TiNi alloys [15] and also has been observed in TiNiPt [5] and TiNiPd [6] shape memory alloys. There may be several causative factors to this behavior, but the largest contribution to the enhanced strain that results on cooling under load is probably due to the nucleation of preferred twin variants, which favor the applied stress. In other words, cooling under load begins to optimize the structure, resulting in a greater fraction of favorably oriented martensite twin variants that can accommodate a larger strain in the sample for a given stress.

Because of the difference in the level of strain developed in the material during loading at room temperature versus cooling under load through the transformation temperature, the first complete heating and cooling cycle at each stress level in the load-bias tests were ignored and only the second complete cycle or hysteresis is plotted in Figs. 10 and 11. Figure 10 shows the results of the strain – temperature behavior of the $Ti_{50.5}Ni_{29.5}Pt_{20}$ 5 mm bar at various stress levels, while Fig. 11 shows comparable data for the 1.1 mm rod. The respective stress for each strain-temperature cycle and the resulting work output are indicated for each set of curves. It is also clear from the data that the $Ti_{50.5}Ni_{29.5}Pt_{20}$ alloy exhibited an increase in transformation temperatures with increasing applied stress, as is common to shape memory alloys.

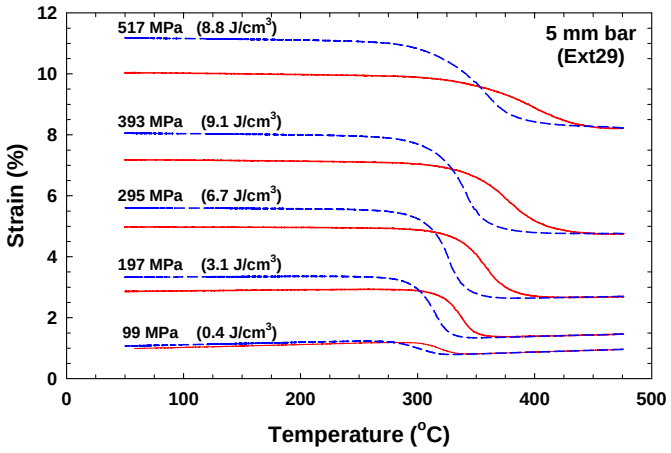

Figure 10: Load-biased, strain temperature response of $Ni_{19.5}Pd_{30}Ti_{50.5}$ 5 mm bar. Solid lines are heating curves and dashed lines are cooling curves. The initial constant stress and resulting work output are indicated for each set of curves.

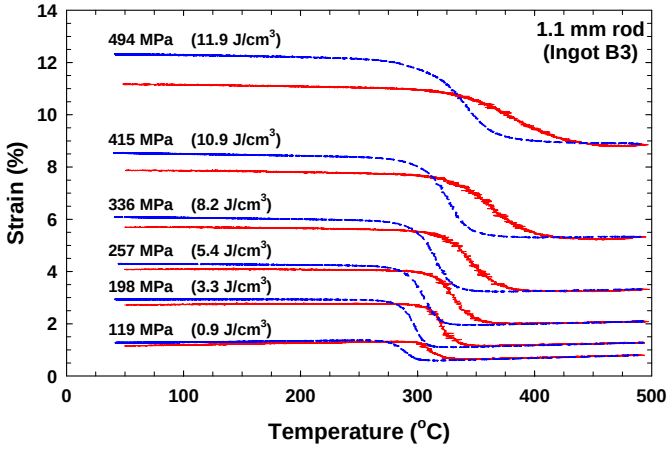

Figure 11: Load-biased, strain temperature response of $Ni_{19.5}Pd_{30}Ti_{50.5}$ 1.1 mm bar. Solid lines are heating curves and dashed lines are cooling curves. The initial constant stress and resulting work output are indicated for each set of curves.

The specific work output was calculated by multiplying the transformation strain on heating by the applied stress for each set of load-bias curves. To more easily compare the behavior of the various forms of the $Ti_{50.5}Ni_{29.5}Pt_{20}$ alloy, the specific work output and transformation strain were plotted versus stress level in Figs. 12 and 13, respectively. Overall, the specific work output increased with increasing stress level until a maximum work output was attained between 400 and 500 MPa depending on the material. The $Ti_{50.5}Ni_{29.5}Pt_{20}$ bar and rod had nearly identical work versus stress characteristics up to a stress level of about 300 MPa. At stresses of 400 MPa or higher, the 1.1 mm rod exhibited better work output due to a higher transformation strain, which is probably due to the refined grain size.

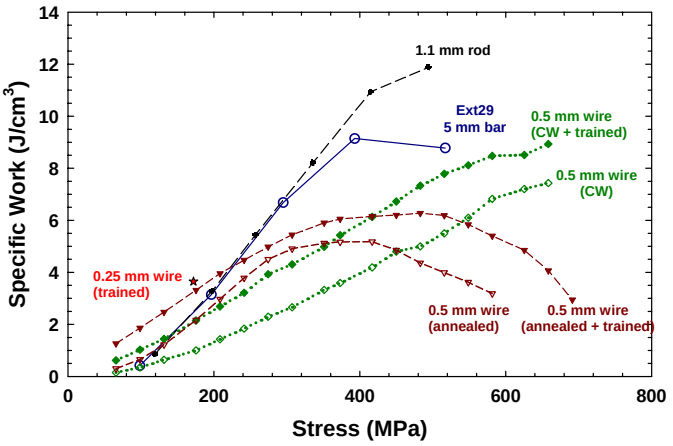

Figure 12: Specific work output as a function of applied stress for various forms of the $Ti_{50.5}Ni_{29.5}Pt_{20}$ alloy.

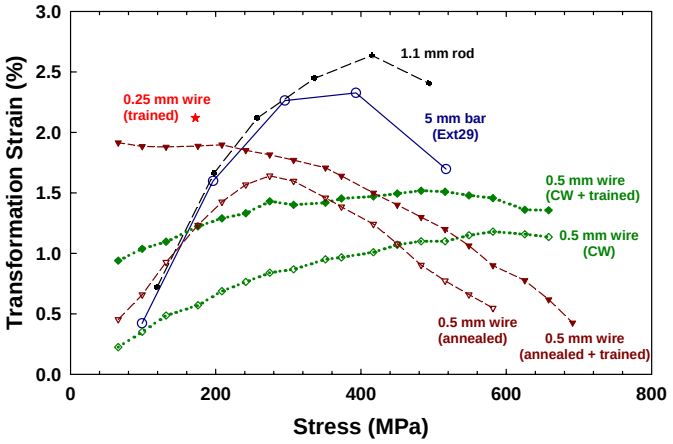

Figure 13: Corresponding transformation strain as a function of applied stress for various forms of the $Ti_{50.5}Ni_{29.5}Pt_{20}$ alloy shown in Fig. 12.

In general, the work output - stress behavior for $Ti_{50.5}Ni_{29.5}Pt_{20}$ was similar to that observed in conventional TiNi alloys. Conventional TiNi alloys exhibit a peak in the work output with maximum values of 10 - 20 J/cm^3 at stresses between 300 – 500 MPa [5,15,16]. This peak in work output is due to competing factors. As the stress level increases, more martensite is favorably aligned during the cooling portion of the cycle so that the available transformation strain on heating increases. But eventually the effect saturates as all the martensite is favorably oriented. Beyond this point as the stress is increased, slip rather than twinning is activated, inhibiting the shape recovery and decreasing the transformation strain. This leads to a peak in transformation strain at some stress level, as shown in Fig. 13. Therefore, even though the applied stress is increasing, the transformation strain eventually begins to decrease and the product of the applied stress and transformation strain, which is work output, also reaches a maximum at some particular stress level.

At nearly every stress level, the strain-temperature curves did not close at the end of the test for the $Ti_{50.5}Ni_{29.5}Pt_{20}$ alloy (Figs. 10 and 11). The amount of plastic deformation that occurred during each cycle can be determined by the strain difference between the heating and cooling curves measured at some temperature well below the transformation temperature and is quite significant at higher stresses. This permanent deformation was due to the larger strain that developed on cooling through the transformation than on heating, as a result of non-recoverable deformation of the martensite. The alloy suffered from plastic or permanent deformation at stresses as low as 100 MPa, even though isothermal monotonic testing would seem to indicate that gross yielding would not be expected in this material at temperatures near the transformation, until stresses in the neighborhood of 200 MPa (Fig. 9) and even that should be due to detwinning.

While the work output of the $Ti_{50.5}Ni_{29.5}Pt_{20}$ alloys falls within the lower range of conventional TiNi alloys, the gross yielding of the alloy at low stresses would prevent the use of this material in most actuator applications. This permanent deformation or dimensional instability is unacceptable since continued thermal cycling of the temperature while under load would cause the material to ratchet or “walk” with each cycle, very quickly exhausting the fatigue life of the sample and eventually resulting in failure. Even if fracture was postponed for a significant number of cycles, changes in length during use of an actuator would cause drifting of the zero point and possible loss of control. The problem with the $Ti_{50.5}Ni_{29.5}Pt_{20}$ and other recently investigated HTSMA systems [6] is that deformation by recoverable twin mechanisms occurs at almost the same stress levels for which non-recoverable mechanisms begin to operate. Therefore, it is necessary to find a method to increase the resistance of the martensite phase to deformation by non-recoverable processes, e.g. dislocation slip.

Very similar behavior, in terms of the occurrence of permanent deformation during load-bias testing, has been observed in $Ti_{50.5}Ni_{19.5}Pd_{30}$ alloys [6]. But recent work on similarly processed but near stoichiometric $Ti_{50}Ni_{30}Pt_{20}$ alloys did not show evidence of significant plastic deformation during thermal cycling under stresses up to 257 MPa [5]. The fact that the $Ti_{50}Ni_{30}Pt_{20}$ exhibits little permanent deformation during load-biased thermal cycling compared to the $Ti_{50.5}Ni_{29.5}Pt_{20}$ would at least seem consistent with reported tensile ductilities for the two materials, which are much

greater for the slightly Ti-rich alloys in this study compared to the near stoichiometric alloys studied previously [5,7,9]. Both results imply that slip is much easier in the Ti-rich alloys compared to near stoichiometric compositions. Consequently, future research will be focused on the effects of stoichiometry on the basic mechanical and work behavior of NiTiPt alloys.

Optimization of Work Output and Dimensional Stability of 0.5 mm Diameter $Ti_{50.5}Ni_{29.5}Pt_{20}$ Wire

Given the progress made thus far in the processing of $Ti_{50.5}Ni_{29.5}Pt_{20}$ alloys, especially wire, and our initial understanding of these materials, we have begun to optimize the alloy specifically for actuator applications. Furthermore, there are a number of things that can be done, alone or in some combination, to reduce or eliminate the amount of plastic deformation observed during load-bias testing in the $Ti_{50.5}Ni_{29.5}Pt_{20}$ alloys. These include the introduction of cold work or some more complicated thermomechanical cycle, solid solution strengthening [2,17], or even in the case of NiTiPt alloys, precipitate strengthening [8].

One of the first steps in understanding the primary factors influencing the properties of the $Ti_{50.5}Ni_{29.5}Pt_{20}$ wire was to determine the effect of cold-drawing on the work behavior of the alloy. Typical load-bias tests on the wire in the cold worked condition (35%) and after a typical recovery anneal (30 min at 600 °C) were performed. The work output - stress response and transformation strain – stress response of the cold worked and annealed materials are shown in Figs. 12 and 13, respectively, which also contain comparable data for the $Ti_{50.5}Ni_{29.5}Pt_{20}$ bar and rod previously discussed. The cold worked material was capable of handling significant stresses but the transformation strains were rather low, generally less than 1%. Therefore, specific work output was low at moderate stress levels. The annealed material had much greater transformation strains and more reasonable work output, but only over intermediate stress levels. However, the issue of dimensional stability during repeated cycling was still a concern.

Therefore, the next step was to reintroduce some plastic deformation back into the material. This was accomplished by cycling the wire through its transformation temperature range, 15 – 20 times, under a stress of 345 MPa and then repeating the load-bias test. This additional thermomechanical cycle was very effective in increasing the transformation strain for even the cold worked wire and benefited the annealed material by both increasing the transformation strain (and thus, work output), especially at the lower stresses and at the same time enhancing the dimensional stability of the material. This improvement in dimensional stability can be seen in Fig. 14. This figure is a plot of cumulative plastic or permanent deformation as a function of the number thermal cycles under a constant load (equivalent to a stress of 172 MPa). Even the cold worked wire was not resistant to plastic deformation. However, through a combination of annealing and training, the $Ti_{50.5}Ni_{29.5}Pt_{20}$ can be made as dimensionally stable or even more so than a commercial “high temperature” nitinol, even though the transformation temperature for the $Ti_{50.5}Ni_{29.5}Pt_{20}$ alloy is over 4 times greater than that of the binary alloy.

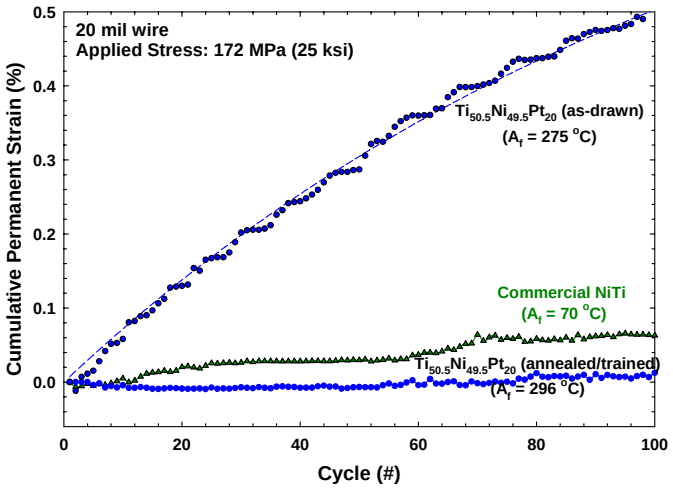

Figure 14: Dimensional stability, measured as cumulative plastic deformation, for $Ti_{50.5}Ni_{29.5}Pt_{20}$ 0.5 mm wire as a function of the number of thermal cycles through the transformation range under a constant load (equivalent to 172 MPa stress) compared to a commercial “high-temperature” nitinol shape memory alloy

While it might not be considered commercially practical to post process $Ti_{50.5}Ni_{29.5}Pt_{20}$ wire by thermally cycling under load, commercial processes providing the same result are being developed by Dynalloy, Inc. A data point for an improved 0.25 mm diameter wire is also shown in Figs. 12 and 13 demonstrating over 2% transformation strain at a stress of 172 MPa for $Ti_{50.5}Ni_{29.5}Pt_{20}$ prepared by commercial processes.

Summary & Conclusions

In the broader search for high-temperature actuator materials, the microstructure and basic mechanical properties of a $Ti_{50.5}Ni_{29.5}Pt_{20}$ alloy have been investigated as a function of various combinations of mechanical and thermal processing. Annealing studies have shown that recovery begins at 450 °C and ends near 600 °C, recrystallization occurs near 700 °C and grain growth occurs at temperatures greater than 700 °C. With this and additional knowledge of the behavior of the $Ti_{50.5}Ni_{29.5}Pt_{20}$ alloy, processing procedures have been successfully developed for the fabrication of bar, thin rod, and even fine diameter wire along with post-processing procedures, for the optimization of this material for actuator applications.

The results have been extremely encouraging. A $Ti_{50.5}Ni_{29.5}Pt_{20}$ alloy has been processed successfully into 0.5 mm and 0.25 mm diameter wire. After post-drawing heat treatment and training, the behavior of the $Ti_{50.5}Ni_{29.5}Pt_{20}$ wire was extremely stable. The transformation temperatures were 270 and 296 °C for the austenite start and finish temperatures, respectively, and the transformation temperatures were stable with respect to repeated thermal cycling to temperatures as high as 450 °C, which corresponds to the temperature at

which recovery begins in this material. The hysteresis was narrow, just 11 °C, making the material ideal for actuator applications requiring active control. After appropriate post-drawing treatment, the transformation strain at 172 MPa (25 ksi) was just over 2% with a corresponding work output at this stress level of nearly 4 J/cm^3 and a maximum work output on the order of 10 - 12 J/cm^3 depending on product form. When appropriately processed the $Ti_{50.5}Ni_{29.5}Pt_{20}$ HTSMA also displays excellent dimensional stability during repeated actuation against a bias stress of 172 MPa and has greater dimensional stability after repeated actuation than commercial "high-temperature" TiNi alloys, even though there is about a 200 °C difference in potential operating temperature.

It is apparent that TiNiPt alloys, for use between 200 and 300 °C, possess attributes that make them promising for high-temperature shape memory applications such as high transformation temperatures, narrow hysteresis, good work output, and reasonable mechanical properties. But further improvements in capability are expected as this TiNi-20Pt HTSMA is carefully optimized by determining the appropriate stoichiometry, combined with the proper wrought processing or combination of cold work and annealing, and other microstructural modifications as required.

Acknowledgments

This work was sponsored by the NASA Aeronautics Program QAT project and Propulsion 21. The authors acknowledge A. Tenteris for a thorough review of the original manuscript and her insightful comments. Inspiration for this work was provided by Nichaela Noebe and is gratefully acknowledged.

References

[1] Mavroidis, C., "Development of Advanced Actuators Using Shape Memory Alloys and Electrorheological Fluids," *Res Nondestr. Eval.*, Vol. 14, (2002), pp. 1-32.

[2] Melton, K., "Ni-Ti Based Shape Memory Alloys," in Engineering Aspects of Shape Memory Alloys, Butterworth-Heinemann, (Boston, 1990), pp. 21-35.

[3] Rasmussen, G. K. *et al.*, "Process for Deposition of Sputtered Shape Memory Alloy Films," U.S. Patent 6,454,913 (2002).

[4] Zhang, J., "Processing and Characterization of High-Temperature Nickel-Titanium-Hafnium Shape Memory Thin Films," PhD Thesis, Michigan State University, (2002).

[5] Noebe, R. *et al.*, "Properties and Potential of Two (Ni,Pt)Ti Alloys for Use as High-Temperature Actuator Materials," *Smart Structures and Materials 2005: Active Materials: Behavior and Mechanics*, SPIE Conf. Proc. Vol. 5761, (2005), pp. 364-375.

[6] Noebe, R. *et al.*, "Properties of a $Ni_{19.5}Pd_{30}Ti_{50.5}$ High-Temperature Shape Memory Alloy in Tension and Compression," *Smart Structures and Materials 2006: Active Materials: Behavior and Mechanics*, SPIE Conf. Proc. Vol. 6170, (2006).

[7] Lindquist, P. G. and Wayman, C. M., "Shape Memory and Transformation Behavior of Martensitic Ti-Pd-Ni and Ti-Pt-Ni Alloys," in Engineering Aspects of Shape Memory Alloys, Butterworth-Heinemann, (Boston, 1990), pp 58-68.

[8] Rios, O. *et al.*, "Characterization of Ternary NiTiPt High-Temperature Shape Memory Alloys," *Smart Structures and Materials 2005: Active Materials: Behavior and Mechanics*, SPIE Conf. Proc. Vol. 5761, (2005), pp. 376-387.

[9] Hosoda, M. *et al.*, "Phase Stability and Mechanical Properties of Ti-Ni Alloys Containing Platinum Group Metals," *Maters Sci. Forum*, Vol. 426-432, (2003), pp. 2333-2338.

[10] DeCastro, *J.A. et al.*, "System-Level Design of a Shape Memory Alloy Actuator for Active Clearance Control in the High-Pressure Turbine," in *Proceedings of the 41st Joint Propulsion Conference and Exhibit*, AIAA, Paper #AIAA-2005-3988, (2005).

[11] Smialek, J., unpublished research, NASA Glenn Research Center, Cleveland, OH., (2005).

[12] Besseghini, S. *et al.*, "Ni-Ti-Hf Shape Memory Alloy: Effect of Aging and Thermal Cycling", *Maters. Sci. Eng.*, Vol. A273-275, (1999), pp. 390-394.

[13] Shimizu, S. *et al.*, "Improvement of Shape Memory Characteristics by Precipitation-Hardening of Ti-Pd-Ni Alloys," *Maters. Lett.*, Vol. 34, (1998), pp. 23-29.

[14] Christian, J. W. and Mahajan, S., "Deformation Twinning," *Prog. Mater. Sci.*, Vol. 39, (1995), pp. 1-157.

[15] Duerig, T. W. *et al.*, "Actuator and Work Production Devices", in Engineering Aspects of Shape Memory Alloys, Butterworth-Heinemann, (Boston, 1990), pp. 181-194.

[16] Cross, W. B. *et al.*, "NITINOL Characterization Study," NASA CR-1433, (1969).

[17] Bigelow, G. et al., "Development and Characterization of Improved High Temperature Shape Memory Alloys by Solid Solution Strengthening and Thermomechanical Processing of NiTiPd Alloys," *SMST 2006: Shape Memory and SuperelasticTechnologies* (current conf. proc.), (2006).